University of
Strathclyde
Glasgow

Strathprints Institutional Repository

http://strathprints.strath.ac.uk/

Simulating the Fast Transport of Water Through Carbon Nanotubes

W.D. Nicholls*, M.K. Borg and J.M. Reese

Department of Mechanical Engineering,
University of Strathclyde, Glasgow G1 1XJ, UK
*william.nicholls@strath.ac.uk

ABSTRACT

Non-equilibrium molecular dynamics simulations are performed to investigate water transport through (7,7) CNTs and to examine how changing the CNT length affects the flow dynamics. We show that fluid flow rates are well in advance of continuum expectations and that this flow enhancement increases with increasing CNT length. This enhancement is related to the internal fluid structure. Water molecules form a tightly packed cylindrical shell inside (7,7) CNTs, with densities nearly 3.5 times that of the water reservoir.

Keywords: carbon nanotubes, molecular dynamics, water flow

1 INTRODUCTION

Recent experiments [1–3] and molecular dynamics (MD) simulations [4–7] have shown that water is transported through carbon nanotubes (CNTs) at unexpectedly high flow rates. The contained fluid structure has also been shown to be dependent upon the CNT diameter: single-file molecule chains at the smallest diameters and high-density structures at larger diameters. The flow of water inside CNTs of diameters below 1.66 nm is non-continuum: the problem cannot be accurately described using conventional continuum fluid mechanics with its associated linear constitutive relations and no-slip boundary conditions [8]. This truly atomistic problem requires a molecular dynamics simulation method.

Very few studies have investigated the effect that varying the CNT length has on the resulting flow rate and fluid structure. In this paper, we use MD simulations to investigate water transport through (7,7) CNTs, which have a diameter of 0.96 nm, with lengths ranging from 2.5 to 25 nm and examine how the change of length affects: fluid flow rate, radial density distributions and flow enhancements over hydrodynamic expectations.

2 SIMULATION METHODOLOGY

Our MD simulations are performed using *mdFoam* [9–12], a parallelised non-equilibrium molecular dynamics solver, that is open-source and available to download from the OpenFOAM website [13]. The motion of molecules is governed by Newton's second law, and the equations of motion are integrated using the Verlet leapfrog scheme. A time-step of 1 fs is used in all the following simulations.

The rigid TIP4P water model is used, which consists of a Lennard-Jones (LJ) interaction potential at the oxygen atom site (O), positive Coulomb charges at the two hydrogen sites (H) and a negative charge at a site M, located a small distance away from O. The O-O LJ interactions use the following parameters: $\sigma_{OO} = 3.154$ Å and $\epsilon_{OO} = 0.6502$ kJ mol^{-1}. The electrostatic point charge values for water are -0.8476e and +0.4238e for the M and hydrogen sites, respectively. The carbon-water interaction is modelled using the LJ potential of Werder *et al.* [14]. Electrostatic and Lennard-Jones interactions are smoothly truncated at 1.0 nm.

The configuration of our pressure-driven flow simulation domain is shown in Fig. 1. Two graphene sheets are positioned at the inlet and outlet of the CNT to form a simplified CNT membrane representation. The CNT and graphene sheets are modelled as rigid structures to speed up the MD runs: this has been reported to be a fair approximation in a previous study [6]. Periodic boundary conditions are employed in the y- and z-directions, while non-periodic boundary conditions are applied in the x-direction: the left-hand boundary is a specular-reflective wall, while the right-hand boundary deletes molecules upon collision. The wall helps control the fluid pressure and density upstream while the deletion patch creates an "open" system [15]. A pressure difference of 200 MPa is applied (see below) across the membrane in all our simulations; such a large pressure difference is required to develop the dynamics of the simulation over a shorter time period due to the large computational cost associated with MD. Berendsen thermostats are applied to both fluid reservoirs to maintain a constant temperature of 298 K and eliminate the contribution of any temperature gradients to the fluid transport. The fluid is not controlled inside the CNT so as not to disturb the dynamics of the contained water molecules.

The upstream pressure is controlled using a proportional-integral-derivative (PID) control feedback loop algorithm, similar to that used in [12], in addition to adap-
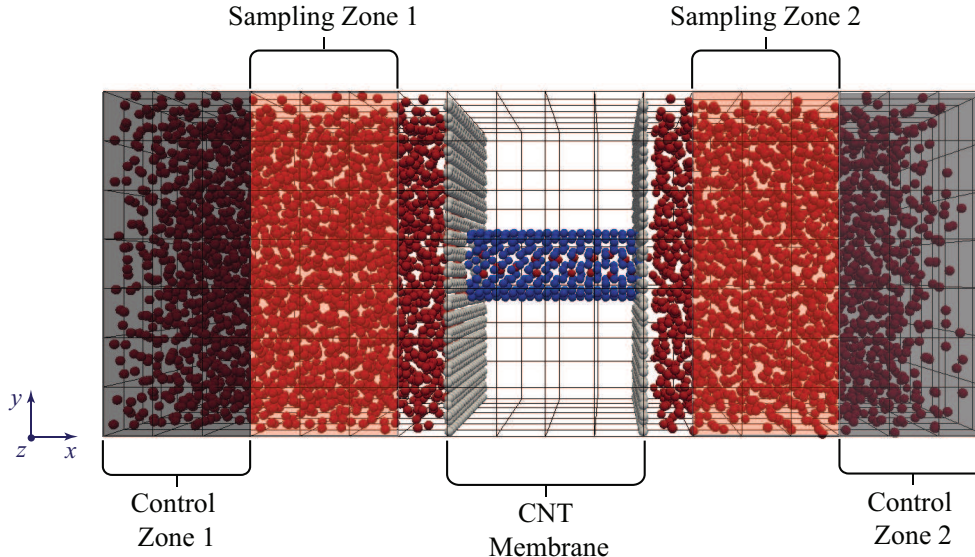
Figure 1: Simulation Domain.

tive control of mass-flux at the inlet. An external force is distributed over all molecules which reside in control zone 1 in order to create the required pressure in the neighbouring sampling region, see Fig. 1. The required external force is calculated using three separate components: a proportional term $\mathbf{f_p}$, an integral term $\mathbf{f_i}$, and a derivative term $\mathbf{f_d}$. This technique is commonly used in modern feedback control systems. The proportional force term is calculated from the pressure error between the measured pressure in the sampling region and the target pressure. The integral force term is calculated using the accumulation of past pressure errors. The derivative force term is calculated using the rate of change of the pressure error. The equation of motion for molecule i located in control zone 1 is then:

$$\mathbf{a_i} = \mathbf{f_i}/m_i + \mathbf{f^{ext}}/m_i, \tag{1}$$

where $\mathbf{a_i}$ is the acceleration of molecule i, $\mathbf{f_i}$ is the interaction force, m_i is the molecule mass and $\mathbf{f^{ext}}$ is the external force given by the sum of all three PID components:

$$\mathbf{f^{ext}} = \mathbf{f_p} + \mathbf{f_i} + \mathbf{f_d}. \tag{2}$$

A mass flux of water molecules is imposed at the inlet of the system in order to compensate for those molecules that leave the system, and to keep the upstream reservoir in a steady thermodynamic state. Our numerical implementation controls density adaptively in the inlet control zone: the target mass density in the control zone is set to the measured fluid density in the sampling region, because the pressure and temperature of the fluid in this region are set at the desired values. The pressure control process helps in establishing a steady and homogeneous density distribution because it forces molecules in and out of the control zone. To improve the stability

of our algorithm, we use relaxation, so that the target density within the control zone is given by:

$$\rho^t = \beta\langle\rho_s\rangle + (1 - \beta)\langle\rho_c\rangle, \tag{3}$$

where $\langle\rho_s\rangle$ is the measured pressure in the sampling zone, $\langle\rho_c\rangle$ is the measured pressure in the control zone, and β is a relaxation parameter (e.g. $\sim$0.5). The number of molecules to insert/delete in the control zone is then:

$$\Delta N = \frac{(\rho^t - \langle\rho_c\rangle)V_c}{m}, \tag{4}$$

where V_c is the volume of the control zone and m is the mass of a molecule. For molecule insertions, the USHER algorithm [16] is used, which searches for a site within the potential energy landscape via a steepest-descent iteration scheme. A molecule is inserted if the potential energy is equal to the cell-averaged potential energy. In this way, the algorithm ensures that the inserted molecule does not overlap with existing water molecules, nor does the local potential energy or temperature change after insertions/deletions. For deletion, the candidate molecule is chosen with its potential energy closest to the cell-averaged potential energy. Momentum and energy conservation steps are also performed after a molecule is inserted/deleted by distributing the added/removed momentum to neighbouring molecules, and updating the pair-forces. The downstream pressure is controlled using a pressure-flux technique, which applies to all molecules in control zone 2 an external force that corresponds to the target. By controlling pressure in this way, it creates an "open" boundary allowing a fluid flux to pass through the system. A key advantage of our pressure control techniques is that the required reservoir pressures can be specified explicitly.
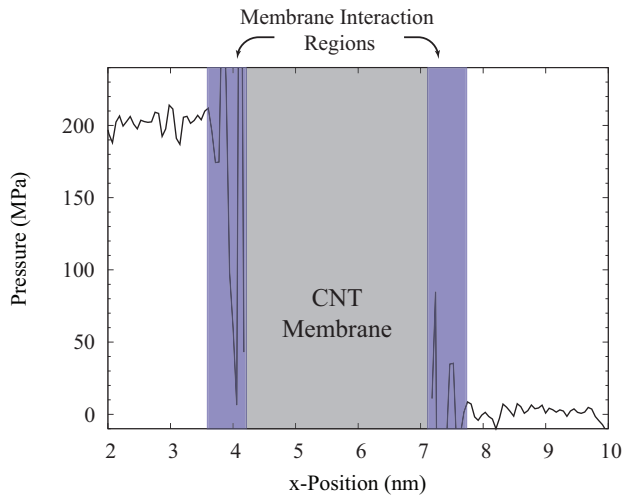
Figure 2: Pressure profile across domain showing the application of a 200 MPa pressure difference.

Four different CNT lengths are investigated: 2.5, 5.0, 12.5, and 25 nm. Initially the CNT is closed while the reservoirs are filled with water molecules and equilibrated to the correct conditions, see Fig. 2. After this initial equilibration, the CNT is opened and allowed to fill naturally. The system is then allowed to run until the number of water molecules inside the CNT remains constant before averaging of properties is performed. The same reservoir conditions are adopted in each simulation run. The maximum variation in the applied pressure difference was measured to be 1.76 MPa.

3   RESULTS AND DISCUSSION

As the fluid transport is non-continuum, the net flow rate is measured by averaging the number of molecules which cross the centre plane inside each CNT over a prescribed time period; molecules which cross in the positive x-direction are counted as positive and those which cross in the opposite direction are counted as negative. The measured mass flow rates are presented in Fig. 3. For all CNT lengths investigated in this study the fluid flow rate remained fairly constant under the same applied pressure difference. This phenomenon has been reported for small changes in nanotube length previously [5], but not for large extensions as presented in this paper. The measured flow rates are compared to predicted, hydrodynamic flow rates via the no-slip Poiseuille relation for flow in a cylindrical pipe:

$$\dot{m} = \frac{\pi r^4 \rho \Delta P}{8 \mu L}, \qquad (5)$$

where r is the radius of the CNT, ΔP is the pressure difference, ρ is the density, μ is the dynamic viscosity, and L is the CNT length. The radius used here is related to the volume which the water can occupy inside a CNT and is half of the carbon to carbon diameter, less σ_{CO}.
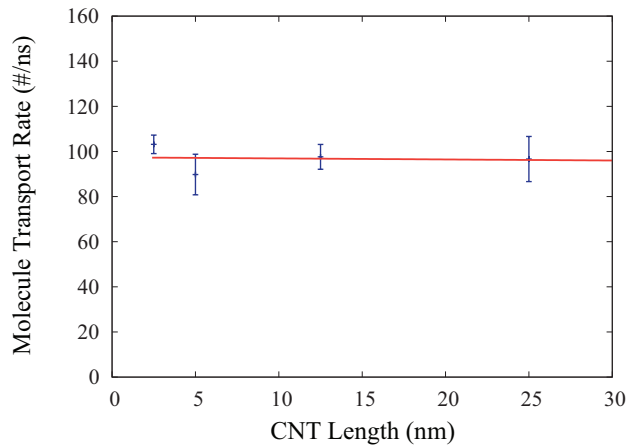

Figure 3: Relationship between flow rate and CNT length under 200 MPa pressure difference.
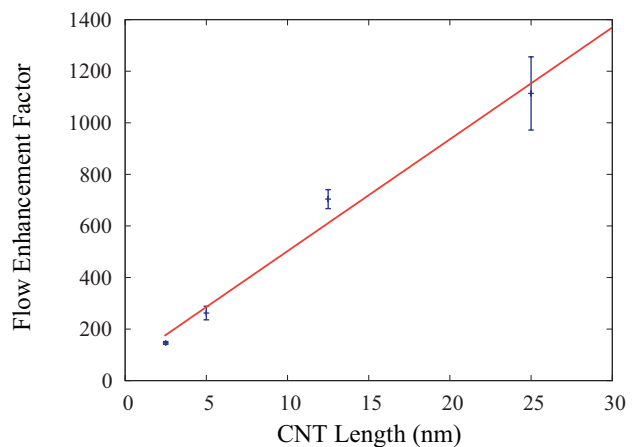

Figure 4: Flow enhancement values for different CNT lengths.

Bulk properties for ρ and μ for water at 298 K are used. The flow enhancement factor, i.e. the ratio of the measured mass flow rate to the hydrodynamic prediction, for each CNT length is shown in Fig. 4. This shows a linear increase with length because the measured mass flow rate stays constant with increasing CNT length, whereas hydrodynamics predicts a linear decrease in mass flow rate with increasing pipe length (if the applied pressure difference is constant).

The average fluid streaming velocity for the different nanotube lengths under the same applied pressure difference are shown in Fig. 5. The fluid velocity is measured at the longitudinal centre of each CNT. As the CNT length increases and the pressure gradient decreases, there is only a slight reduction in the fluid velocity. Thomas and McGaughey [8] measured fluid velocities of 4 nm/ns for the same diameter of CNT under much smaller pressure gradients and found the relationship between the velocity and applied pressure gradient to be non-linear. This suggests that at higher pressure gradients the fluid velocity may tend towards a maximum value for a given CNT diameter; 15 nm/ns for this
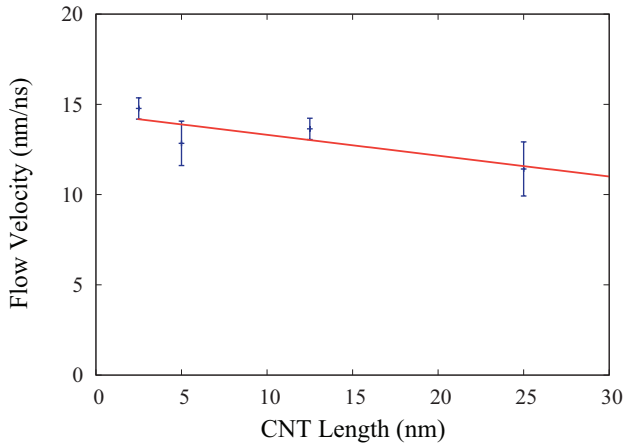
Figure 5: Variation of flow velocity with CNT length under 200 MPa pressure difference.
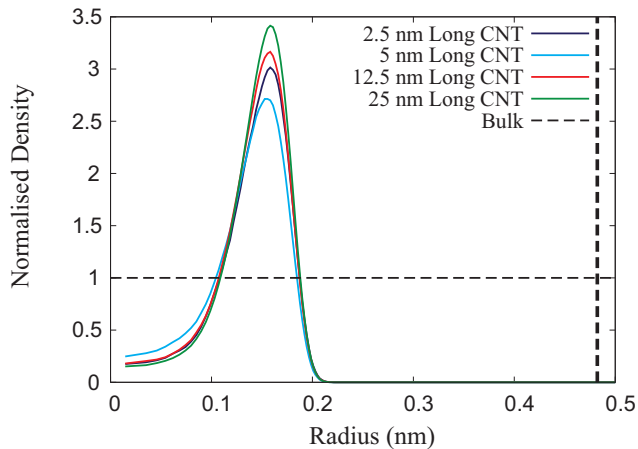

Figure 6: Radial density distributions normalised with the reservoir density for CNTs with different lengths. The vertical dashed line indicates the position of the CNT surface.

case. This extraordinary non-continuum transport behaviour may be related to the internal fluid structure, which we now describe.

The fluid structure within the CNTs is investigated by measuring the mean radial density at the longitudinal centre of each CNT. Figure 6 shows that water contained within each CNT forms tightly-packed cylindrical shells, whose densities are dependent upon the nanotube length. The maximum density of the water in these shells in the longer CNTs is greater than that in the shorter CNTs, with the 25 nm long CNT having a maximum of almost 3.5 times that of the water reservoir density. The distance between where the peak density of the cylindrical shells occurs and the CNT surface corresponds to the interaction length of the Lennard-Jones potential between the carbon and oxygen atoms. Although the fluid velocity decreases with increasing CNT length, the fluid density at the centre increases, which means the flow rate stays constant with increasing CNT length. The density profiles measured at the longitudi-

nal centre of each CNT vary with length: the maximum density in a 25 nm CNT is higher than that in a 2.5 nm CNT. This suggests that the structure of the transported water is able to develop in longer CNTs i.e. CNTs with greater lengths optimise the fluid molecular packing for significant flow rate enhancements.

4   CONCLUSIONS

The results of non-equilibrium MD simulations have been reported on water transport through (7,7) CNTs, in particular, how changing the CNT length affects the internal flow dynamics. Using new fluid pressure MD control techniques we have shown that (i) under the same applied pressure difference an increase in CNT length can result in increased flow enhancements over continuum expectations, (ii) water molecules form a tightly packed cylindrical shell inside (7,7) CNTs with densities reaching nearly 3.5 times that of the water reservoirs for certain CNT lengths, and (iii) the internal fluid structure is dependent upon the CNT length: longer CNTs form water structures with a greater density.

5   ACKNOWLEDGEMENTS

REFERENCES

[1] M. Majumder, N. Chopra, R. Andrew, and B. J. Hinds. Nanoscale hydrodynamics: enhanced fluow in carbon nanotubes. *Nature*, 438:44, 2005.

[2] J. K. Holt, H. G. Park, Y. Wang, M. Stadermann, A. B. Artyukhin, C. P. Grigoropoulos, A. Noy, and O. Bakajin. Fast mass transport through sub-2-nanometer carbon nanotubes. *Science*, 312(5776):1034–1037, 2006.

[3] M. Whitby, L. Cagnon, M. Thanou, and N. Quirke. Enhanced fluid flow through nanoscale carbon pipes. *Nano Letters*, 8(9):2632–2637, 2008.

[4] J. A. Thomas, A. J. H. McGaughey, and O. Kuter-Arnebeck. Pressure-driven water flow through carbon nanotubes: insights from molecular dynamics simulation. *International Journal of Thermal Sciences*, 49(2):281–289, 2010.

[5] B. Corry. Designing carbon nanotube membranes for efficient water desalination. *Journal of Physical Chemistry B*, 112(5):1427–1434, 2008.

[6] S. Joseph and N. R. Aluru. Why are carbon nanotubes fast transporters of water? *Nano Letters*, 8(2):452–458, 2008.

[7] M. E. Suk, A. V. Raghunathan, and N. R. Aluru. Fast reverse osmosis using boron nitride and carbon nanotubes. *Applied Physics Letters*, 92(13):133120, 2008.

[8] J. A. Thomas and A. J. H. McGaughey. Water flow in carbon nanotubes: transition to subcontinuum transport. *Physical Review Letters*, 102(18):184502, May 2009.

[9] G. B. Macpherson, N. Nordin, and H. G. Weller. Particle tracking in unstructured, arbitrary polyhedral meshes for use in cfd and molecular dynamics. *Communications in Numerical Methods in Engineering*, 25(3):263 – 273, 2009.

[10] G. B. Macpherson, M. K. Borg, and J. M. Reese. Generation of initial molecular dynamics configurations in arbitrary geometries and in parallel. *Molecular Simulation*, 33(15):1199 – 1212, 2008.

[11] G. B. Macpherson and J. M. Reese. Molecular dynamics in arbitrary geometries: Parallel evaluation of pair forces. *Molecular Simulation*, 34(1):97 – 115, 2008.

[12] M. K. Borg, G. B. Macpherson, and J. M. Reese. Controllers for imposing continuum-to-molecular boundary conditions in arbitrary fluid flow geometries. *Molecular Simulation*, 36(10):745 – 757, 2010.

[13] OpenCFD Ltd. http://www.openfoam.com, 2011.

[14] T. Werder, J. H. Walther, R. Jaffe, T. Halicioglu, and P. Koumoutsakos. On the water-carbon interaction for use in molecular dynamics simulations of graphite and carbon nanotubes. *Journal of Physical Chemistry B*, 107(41):1345–1352, 2003.

[15] E. G. Flekkøy, R. Delgado-Buscalioni, and P. V. Coveney. Flux boundary conditions in particle simulations. *Physical Review E*, 72(2):026703, 2005.

[16] G. D. Fabritiis, R. Delgado-Buscalioni, and P. V. Coveney. Energy controlled insertion of polar molecules in dense fluids. *Journal of Chemical Physics*, 121(24):12139–12142, 2004.